Pairing Measurements of the Water Vapor Isotope Ratio with Humidity to Deduce Atmospheric Moistening and Dehydration in the Tropical Midtroposphere

DAVID NOONE

Department of Atmospheric and Oceanic Sciences, and Cooperative Institute for Research in Environmental Sciences, University of Colorado, Boulder, Colorado

(Manuscript received 26 October 2010, in final form 6 November 2011)

ABSTRACT

Measurements of the isotope ratio of water vapor (expressed as the δ value) allow processes that control the humidity in the tropics to be identified. Isotopic information is useful because the change in δ relative to the water vapor mixing ratio (q) is different for different processes. The theoretical framework for interpreting paired q–δ data is established and based on a set of simple models that account for mixing and a range of condensation conditions. A general condensation model is derived that accounts for cloud precipitation efficiency and postcondensation exchange. Using data from the Tropospheric Emission Spectrometer (TES), aspects of subtropical hydrology are characterized by the match between theoretical curves and observed displacement in q–δ space. The subtropics are best described as the balance between drying associated with (mostly horizontal) transport of dry air from high latitudes and moistening by clouds with low precipitation efficiency. In the western Pacific moistening involves the import of air into which raindrops have evaporated and is identified by ''super-Rayleigh'' isotopic distillation. In the dry subtropics, the observations are consistent with the condensation–advection explanation for the humidity minimum but also reflect details of the cloud processes and moistening by high humidity filaments of tropical origin. In spite of limitations of the TES data, the success of the analysis highlights the value of using isotopic data in analysis of tropospheric moisture budgets and the role water isotopic ratio measurements can play in identifying mechanisms associated with large-scale changes in atmospheric humidity.

1. Introduction

Water vapor in the earth's atmosphere is an important part of the climate system because of its role in absorbing terrestrial radiation, allowing the formation of clouds and heating the atmosphere (e.g., Schneider et al. 2010; Sherwood et al. 2010). The mean relative humidity (RH) of a geographic region characterizes aspects of the atmospheric hydrology because of how the types of processes that are likely to occur in regions that are either near or far from saturation differ. Since the isotopic composition of water vapor reflects the history of exchange processes (e.g., Payne et al. 2007; Worden et al. 2007; Noone 2008; Risi et al. 2008; Wright et al. 2009; Sayres et al. 2010), measurements of the isotopic composition in both high and low RH regions in the troposphere also give an indication of which processes dominate the moisture budget. The aim of this paper is to use measurements of the HDO/H_2O isotope ratio (R) to identify processes that govern the moisture balance in the subtropics. This can only be achieved once an adequate theory is established to link the observed isotope ratio to different processes that contribute to the water vapor budget.

Low humidity conditions in the subtropics can be maintained with dehydration by quasi-horizontal large-scale eddy mixing, and simple advection–condensation models can reproduce many of the observed features of the humidity field (Sherwood 1996a; Salathe and Hartmann 1997; Pierrehumbert and Roca 1998; Galewsky et al. 2005; Cau et al. 2007; Hurley and Galewsky 2010). Pierrehumbert et al. (2007) suggested the reason for the efficient dehydration is the strong temperature variability in the extratropics that controls the condensation. Schneider et al. (2006) showed that, in zonal mean statistics, water vapor removed from the subtropics by adiabatic eddies dominates the drying of the subtropical lower troposphere. Poleward eddy moisture transport is often observed in association with

Corresponding author address: David Noone, Department of Atmospheric and Oceanic Sciences, Campus Box 216, University of Colorado, Boulder, CO 80309-0216.
E-mail: dcn@colorado.edu

DOI: 10.1175/JCLI-D-11-00582.1

© 2012 American Meteorological Society

narrow spatial-scale filaments (Newell et al. 1992; Zhu and Newell 1998), while the cold flank of eddies are dry and transport low humidity air toward the equator (Yang and Pierrehumbert 1994). However, the advection–condensation approach often neglects differences in cloud processes, the role of cloud-scale organization, and the possibility that dry air can be rehydrated by evaporation of cloud ice or liquid formed during the time of last saturation (Sherwood et al. 2010). The role of shallow cumulous in moistening, for instance, is well known (Yang and Pierrehumbert 1994; Bretherton et al. 1995; Sherwood 1996a; Couhert et al. 2010). Bony and Emanuel (2005) note that the precipitation efficiency, which is defined as the fraction of condensed cloud water that is converted to precipitation, is a critical parameter in setting the tropospheric humidity. The precipitation efficiency is a convenient bulk measure of cloud microphysics and cloud macrophysical behavior yet is not readily measurable.

The isotopic composition of water vapor provides insight into the origins of water and aspects of cloud processes because of fractionation during phase change. Both equilibrium fractionation (that allows vapor pressure–dependent separation between heavy and light isotopologues) and rate-dependent kinetic fractionation (associated with diffusion during condensation and evaporation) lead to distinct isotopic signatures in different water sources and exchange processes (e.g., Dansgaard 1964; Gat 1996). The large-scale distribution of water vapor isotope ratio is conveniently viewed as a balance between the depleting effects of condensation (say, as in a Rayleigh processes) and the mixing of air masses with vapor of differing isotopic composition during large-scale transport and the enriching effects during supply from a boundary layer source (Noone 2008; Galewsky and Hurley 2010). However, there has been no observational demonstration that this is quantitatively robust.

Beyond an advection–condensation description, the isotope ratios capture the microphysical history because the condition under which condensation occurs influences the fractionation. For instance, evidence for remoistening by condensate evaporation stands out in the isotope ratio because of the disequilibrium exchange between falling raindrops and ambient environmental water vapor (Lawrence et al. 2004; Worden et al. 2007; Risi et al. 2008; Wright et al. 2009; Field et al. 2010). Therefore, while using isotopic signatures to identify cloud processes holds potential to evaluate the influence of cloud microphysical controls on the humidity, a new theoretical approach to link isotopic observations to underlying mechanisms is required. While many simple models for isotopic mixing and fractionation exist for specific isolated cases (e.g., Dansgaard 1964; Craig and Gordon 1965; Gedzelman 1988; Ciais and Jouzel 1994; He and Smith 1999a; Gat 2000; Noone et al. 2011), a compilation of a set of isotope models is more appropriate for the atmospheric hydrology where many different processes may act within, say, a season or along some transport pathway. Any set of models should be derived from a common expression of mass conservation, be consistent with expected meteorological controls, and reflect the balance between many processes.

This paper establishes a theoretical basis for using isotope ratio observations paired with the water vapor mixing ratio to identify different water sources, condensation processes, and transport pathways in the troposphere, and then use the isotopic measurements to infer dominant influences on the moisture budgets in the tropics and subtropics. Specifically, we seek to identify 1) how clouds and turbulent-scale mixing processes modify the simple depiction that results from condensation at the saturation temperature (as in a Rayleigh process) with subsequent advection, 2) if remoistening by rain evaporation is a widespread feature of the tropics, 3) what proportion of the moisture comes from evaporation of falling ice and liquid precipitation formed in deep convection versus water lofted and detrained from shallower convection, and 4) if moistening by cloud processes is principally associated with detrainment or evaporation of shallow clouds. Tropical regions with high and low relative humidity are examined since these areas have characteristically different hydroclimates. Estimates of the HDO to H_2O isotope ratio, R, in the lower mid-troposphere are obtained from infrared emission spectra measured by the Tropospheric Emission Spectrometer (TES) on the *Aura* spacecraft. Given known limitations in the quality and sampling biases in remotely sensed data, a further objective is to evaluate to what degree existing isotope ratio data can provide practical information for constraining atmospheric hydrology.

2. Mass balance constraints on paired observations

a. Isotope exchanges from budget constraints

The isotopic composition is given in ''delta'' notation, which is a normalized difference from the isotope ratio from the isotope ratio of Vienna Standard Mean Ocean Water (R_s): $\delta = R/R_s - 1 \approx \ln(R/R_s)$. Since dehydration and moistening processes influence δ at the same time as q, modeling how δ changes relative to q under different assumptions gives the framework for interpreting paired isotope–humidity observations. Specifically, it is the change in δ relative to change in q, rather than the change in δ alone, which provides the unique information that we

wish to exploit. The theory developed here extends previous work (e.g., Keeling 1958; Merlivat and Jouzel 1979; Gedzelman 1988; Ciais and Jouzel 1994; Gat 1996; He and Smith 1999b; Gat 2000) and is based on a set of simple models that arise from mass balance.

For a homogeneous air parcel, the mass balance for H_2O or HDO vapor mixing ratio (q or q_D) is

$$\frac{dq}{dt} = M + S - C + X = \dot{q}. \tag{1}$$

In the absence of sources of sinks, the mixing ratio and the isotope ratio are conserved. The water source S captures the influx of water from the boundary layer (including detrainment) and is a vertical mixing process. Horizontal mixing is M. Condensation, C, occurs when the air mass is saturated. Evaporation of precipitation is a source X and occurs when hydrometeors fall through subsaturated air. Newly condensed water may remain as cloud liquid or fall as precipitation depending on the bulk cloud precipitation efficiency. Precipitation efficiency, ε, is defined as the fraction of condensation that falls as precipitation (i.e., $P = \varepsilon C$). The remaining condensation, $(1 - \varepsilon)C$, is the production of cloud liquid. Including the rainfall efficiency is a key aspect of the present analysis.

An expression similar to (1) can be written for q_D where isotopic counterparts to S, C, X, and M differ because of fractionation and the isotopic composition of the source water (e.g., Noone and Sturm 2010). Given different assumptions, as depicted in Fig. 1, integrating the budget equation, (1), leads to different relationships of the form $\delta = \delta(q)$ that can be plotted on a q–δ diagram, which is used as the basis of the theoretical framework for water vapor measurements. The approach taken here can also be applied to the case of total water (i.e., $q + l$) when observations are taken in the region of clouds. In the development that follows condensation, processes and sources associated with mixing are considered separately.

1) Condensation processes

With no water sources (M and S set to zero, as in Figs. 1a–c), (1) is written for both q and q_D and a general condensation model is derived for a homogenous air mass as a function of ε. The governing equations are

$$dq + dl + dr = 0, \tag{2}$$

where q is the vapor, l is the mass of cloud liquid, r the mass of rain, and

$$\begin{aligned} dq &= -C \\ dl &= C - P \\ dr &= P. \end{aligned} \tag{3}$$

The (constant) precipitation efficiency ε is introduced such that the precipitation rate is proportional to the condensation rate, $P = \varepsilon C$, and so $dl = -(1 - \varepsilon)dq$. Since ε is constant, integration from some initial state (denoted with subscript 0) gives

$$l = l_0 + (1 - \varepsilon)(q_0 - q). \tag{4}$$

Cloud liquid remains in isotopic equilibrium with the vapor and new precipitation forms from cloud water (e.g., by coalescence) without further fractionation (Merlivat and Jouzel 1979; Ciais and Jouzel 1994). That is

$$dq_D + dl_D + dr_D = 0, \tag{5}$$

$$\frac{l_D}{l} = \alpha\frac{q_D}{q}, \quad \text{and} \tag{6}$$

$$\frac{d(q_D + l_D)}{d(q + l)} = \alpha\frac{q_D}{q}. \tag{7}$$

Subscript D denotes the heavy isotopologue. Equilibrium, (6), can be written as the following:

$$\frac{q_D}{q} = \frac{q_D + l_D}{q + \alpha l}. \tag{8}$$

Substituting (8) into (7) and using (4) to eliminate l, the system is

$$\frac{d(q_D + l_D)}{q_D + l_D} = \alpha\varepsilon\left\{\frac{1}{[1 - \alpha(1 - \varepsilon)]q + \alpha[l_0 + (1 - \varepsilon)q_0]}\right\}dq. \tag{9}$$

One may integrate immediately and substitute to find changes in the isotope ratio. Further simplifying using (6) and (4) to eliminate l_D, and applying the product rule, a more compact differential form for the isotope ratio R is

$$\frac{d\ln R}{d\ln q} = \frac{\alpha[l_0 + q_0 + \varepsilon(q - q_0)]}{q + \alpha[l_0 + (1 - \varepsilon)(q - q_0)]} - 1. \tag{10}$$

Upon integrating

$$\delta - \delta_0 \approx \ln\left(\frac{R}{R_0}\right) = \left[\frac{\alpha\varepsilon}{1 - \alpha(1 - \varepsilon)} - 1\right] \times \ln\left[\frac{\alpha l_0 + q - \alpha(1 - \varepsilon)(q - q_0)}{\alpha l_0 + q_0}\right]. \tag{11}$$

Notice α is assumed constant in this derivation, which is only valid for small changes in q, but is readily relaxed in

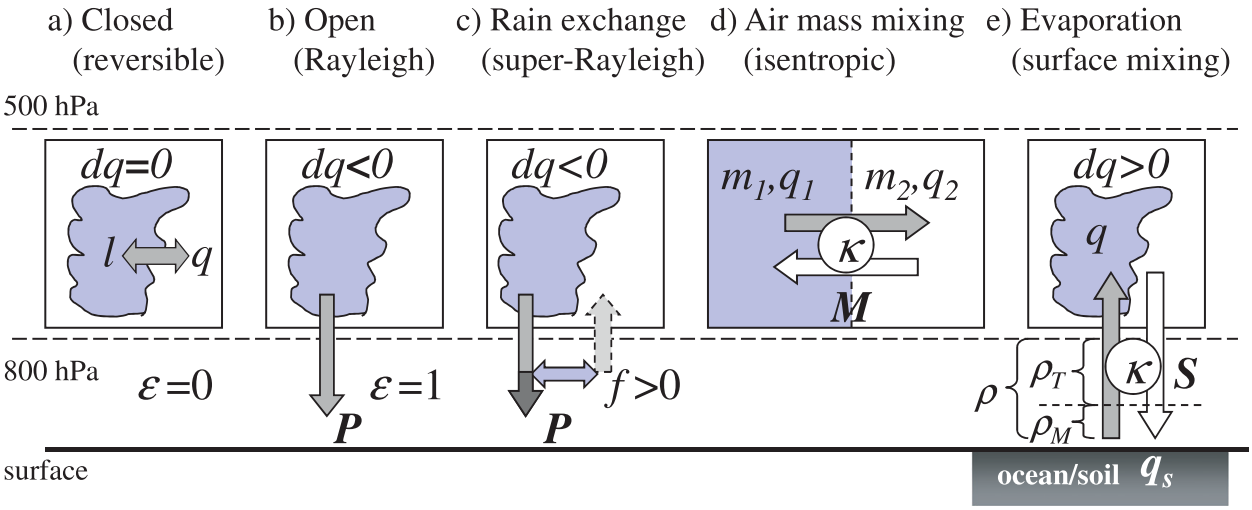

FIG. 1. Depiction of simple Lagrangian mass balance models applied to the atmosphere. Shading indicates higher isotopic δ values, and arrows indicate the fluxes of principal importance. See text for explanation of symbols. (a) Reversible moist adiabatic processes retain total water mass with the liquid and vapor in thermodynamic equilibrium, while (b) removal of water can occur as in a Rayleigh process or (c) accounting for postcondensation exchange as liquid drops fall and evaporate. (d) Airmass mixing represents an exchange between two reservoirs at a rate given by an exchange coefficient. (e) Evaporation is a special case of mixing where the source is the ocean or water in the land surface and essentially infinite. In this case, the total exchange depends on both turbulent and molecular resistance indicated by the symbols ρ.

numerical evaluation.[1] Further, α is the effective fractionation that need not be identical to the equilibrium fractionation factor α_e, as described below. A benefit of (11) is that the cloud physics are described by two parameters: α and ε.

If all condensation is removed ($\varepsilon = 1$), as in a pseudoadiabatic process (or is otherwise isolated from the vapor with condensation to ice), (11) reduces to the well-known Rayleigh (1902) distillation model (e.g., Craig et al. 1963; Dansgaard 1964; Sharp 2006):

$$(\delta - \delta_0) \approx \ln\left(\frac{R}{R_0}\right) = (\alpha - 1)\ln\left(\frac{q}{q_0}\right). \qquad (12)$$

The fractionation factor can be chosen as the equilibrium fractionation factor at the dewpoint temperature by assuming the mixing ratio q is the saturation value at the condensation pressure (taken as 650 hPa, which is typical for TES data). The geometric result is that (12) describes a logarithmic trajectory in the q–δ plane, as in Fig. 2, where an initial point is chosen at 80% relative humidity over an ocean at 300 K. The fractionation factor is for liquid when dewpoint temperature is above 263 K (i.e., $q = 3.96$ mmol mol^{-1}), and otherwise is for ice. A frost point of 263 K is chosen to account for the coexistence of ice and liquid as in the mixed phase model of Ciais and Jouzel (1994). The curve in Fig. 2 is constructed by applying (12) over many small steps to account for the temperature dependence of α(since $d\alpha/dT = -1.4‰\ \mathrm{K}^{-1}$ at 10°C).

A reversible moist adiabatic process is one in which condensation is slow and liquid condensate remains with the vapor (i.e., precipitation efficiency $\varepsilon = 0$, Fig. 1a). This occurs when the drop size is small (e.g., cloud droplets or light drizzle). From (6), and noting conservation gives $q_0 = l + q$, the model reduces to the "closed-system" model (e.g., Jouzel 1986):

$$\delta - \delta_0 = (\alpha_e - 1)\left[\frac{q - q_0}{q - \alpha_e(q - q_0)}\right]. \qquad (13)$$

Since $\ln(x/x_0) = -\ln(x_0/x) \approx -[(x_0/x) - 1]$, an approximation to (13) is

$$\delta - \delta_0 \approx (\alpha_e - 1)\left(\frac{q}{q_0} - 1\right), \qquad (14)$$

which reveals δ is linearly dependent on q. Figure 2 shows that the evolution of (13) is weakly nonlinear because of the dependence of α_e on (dewpoint) temperature. Below the frost point, low diffusivity of H_2O and HDO in ice prevents this reversible behavior because the condensate

[1] The function is finite for all values of ε and α. For the special case of $\varepsilon = 1 - (1/\alpha)$,which gives $\ln(1) = 0$, stability can be demonstrated analytically using l'Hôpital's rule. However, care should be taken in numerical evaluation to check the results since the factor in front of the logarithm tends toward infinity.

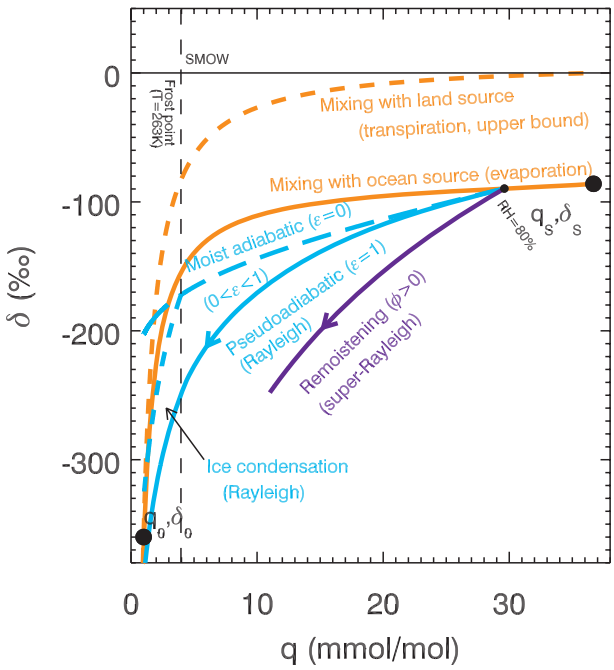

FIG. 2. Theoretical predictions of the evolution of δ as a function of q. A Rayleigh curve represents a pseudoadiabatic process and is shown as the solid cyan curve assuming an original air mass that has 80% relative humidity relative to equilibrium with an ocean source marked at point q_s, δ_s with an assumed temperature of 300 K. The case of a reversible moist adiabatic process is shown as the dashed cyan curve assuming the same origin, with a transition to a Rayleigh process below 263 K when condensation is to ice and irreversible. The case of remoistening associated with isotopic exchange as raindrops evaporate into a subsaturated layer is shown in purple. The solid orange curve shows evaporation as mixing with vapor in equilibrium with the ocean surface, with an assumed dry end member at q_0, δ_0. The dashed orange curve shows the evolution associated with a more enriched source, such as terrestrial transpiration, and represents an upper bound. Mixing between any two arbitrary points will trace hyperbolic mixing lines.

is effectively isolated from the vapor and the evolution again follows a Rayleigh process for temperatures below the frost point.

In the case where some fraction of the liquid condensate is retained (i.e., $0 < \varepsilon < 1$), the q–δ evolution during condensation will follow a curve that lies between the two extreme cases shown in Fig. 2. The condensation model allows the isotope ratio to be used to trace irreversible water loss during condensation in ice-free clouds via ε.

2) PARTIAL EVAPORATION OF FALLING RAIN

Falling precipitation can evaporate and undergo isotopic exchange (Fig. 1c). This can lead to an isotopic ratio of the precipitation exceeding that at equilibrium and leave the remaining vapor more depleted (Dansgaard 1964; Stewart 1975; Rozanski et al. 1992). The isotopic exchange near raindrops brings the raindrop isotope ratio toward equilibrium with the ambient vapor (Stewart 1975; Jouzel 1986; Lee and Fung 2008). The isotope ratio of the evaporative flux is

$$\frac{X_D}{X} = \alpha_k \left(\frac{\alpha_e^{-1} R_r - h_r R_b}{1 - h_r} \right), \tag{15}$$

where h_r is the relative humidity near the drop ($0 < h_r < 1$), α_k is the kinetic fractionation that depends on the diffusivity of H_2O and HDO in air and h_r (via a ventilation factor at the liquid–air interface of the raindrop), R_r is the isotope ratio of rain, and R_b is the isotope ratio of the vapor through which the drops fall. A similar expression that more explicitly accounts temperature changes that accompany the latent heat exchange during evaporation can be used to better quantify the effective kinetic fractionation [note the ratio of Eqs. (B14) and (B7) given by Blossey et al. (2010)]. Such expressions are readily evaluated in atmospheric models where the ambient vapor is simulated (Hoffmann et al. 1998; Noone and Simmonds 2002; Lee et al. 2007; Bony et al. 2008; Risi et al. 2008; Yoshimura et al. 2008). For single-altitude measurements, like the TES data, the lack of information below the condensation height requires additional assumptions to be made.

Using TES data, Worden et al. (2007) applied the simplest assumption that exchange proceeds as a batch distillation of the raindrops (i.e., large drops falling through very low humidity air, and so $h_r \approx 0$). This is an upper bound. With the isotope ratio of the raindrops higher, the isotope ratio of vapor remaining becomes lower. That is, the difference between the isotope ratio and the original vapor is greater than equilibrium fractionation predicts (i.e., $\alpha > \alpha_e$). In the case $h_r = 1$, (15) is poorly defined (since $X = 0$), but isotopic exchange is possible ($X_D \neq 0$). The case of $h_r = 1$ suggests thermodynamic equilibrium and $R_r = \alpha_{eq} R_b$, which provides another bound (also see discussion by Bony et al. 2008). If the isotope ratio of the ambient vapor is the same as the original vapor, then there would be no change in isotope ratio of the rain drop or the vapor. Therefore, the objective is to determine by how much the isotope ratio of rain exceeds the isotope ratio in equilibrium with the vapor and then to write an expression for the effective fractionation α that can be used in (11).

Since the isotopic composition of the low-level vapor, the size distribution of rain drops, and humidity are not readily known from paired q–δ observations, the effective fractionation is defined in a simple parameterized form as

$$\alpha = (1 + \phi)\alpha_e, \tag{16}$$

where ϕ is the degree to which α deviates from equilibrium. Physical insight into ϕ may be obtained by considering the case when some fraction of the precipitation f evaporates and remains in the atmosphere ($X = fP$, where $0 \leq f \leq 1$). For the case $\varepsilon = 1$ (for simplicity),

$$\frac{dq}{dt} = -(1 - f)P$$
$$\frac{dq_D}{dt} = -\alpha_e(1 + \phi)(1 - f)RP, \tag{17}$$

and with the aid of (15)

$$\phi = \frac{f}{(1 - f)}\left\{1 - \frac{\alpha_k}{\alpha_e}\left[\frac{1 - h_r\left(\frac{R_b}{R}\right)}{1 - h_r}\right]\right\}. \tag{18}$$

Inspection reveals that $\phi > 0$ (i.e., $\alpha > \alpha_e$), requires $R_b > R$, and the rate of change of q_D will be greater than at equilibrium. Therefore the "slope" of the curves in the q–δ plane is steeper than the Rayleigh curve. Rain evaporation curves are labeled "super-Rayleigh" in Fig. 2. Taking values of $f = 0.1$, $h_r = 0.8$, and $R_b/R = 1.2$ gives $\phi \sim 0.1$, as plotted, although ϕ will be reduced as the isotope ratio of the boundary layer changes (see Bony et al. 2008). While many processes can produce sub-Rayleigh trajectories (retention of cloud water, near complete evaporation of rain, and airmass mixing), partial rain evaporation appears to be a process that gives a super-Rayleigh path. (One can imagine certain chemical processes and surface water sources with very low isotope ratios that could also give rise to similar outcomes, but these are uncommon.). Exchange during rain evaporation can be identified in data if it falls below the Rayleigh curve ($\alpha = \alpha_e$) and exhibits the super-Rayleigh behavior.

3) AIRMASS MIXING

Mixing models for isotope ratios (e.g., Gedzelman 1988; He and Smith 1999a; Dessler and Sherwood 2003; Lee et al. 2007; Wen et al. 2008; Noone et al. 2011), as in Fig. 1d, receive less attention than condensation models yet are more relevant in many cases. Mixing tends to bring both q and δ toward a final well-mixed state $(\hat{q}, \hat{\delta})$, which is the mass-weighted mean of the two initial air masses. Specifically,

$$\hat{q} = \left(\frac{m_1 q_1 + m_2 q_2}{m_1 + m_2}\right) \tag{19}$$

and similarly for $\hat{R}$ to give $\hat{\delta}$, where the subscripts 1 and 2 denote the two air masses and m is the mass. The asymptotic approach to this state is

$$\frac{dq}{dt} = -\kappa(\hat{q} - q)$$
$$\frac{dRq}{dt} = -\eta\kappa(\hat{R}\hat{q} - Rq), \tag{20}$$

where κ is an exchange coefficient and η accounts for slower diffusion of heavier nuclides. (For most atmospheric mixing one may take $\eta = 1$ for purely turbulent mixing.) For air of constant mass, integration gives

$$q = q_0 + q_F$$
$$Rq = R_0 q_0 + R_F q_F, \tag{21}$$

where

$$q_F = (\hat{q} - q_0)(1 - e^{-Kt})$$
$$R_F = \frac{\hat{R}\hat{q} - R_0 q_0}{\hat{q} - q_0}, \tag{22}$$

and the subscript F denotes the flux into the volume of interest. Upon rearranging and converting to δ notation, the mixing model is

$$\delta = \frac{R}{R_s} - 1 = q_0(\delta_0 - \delta_F)\frac{1}{q} + \delta_F. \tag{23}$$

The evolution follows a hyperbolic path in the q–δ plane, as shown in Fig. 2. A derivation based on a diffusion equation is a more general case developed elsewhere and yields the same result, which highlights the robustness of this hyperbolic relationship (Noone et al. 2011).

The hyperbolic shape fundamentally arises from the definition $R = q_D/q$, with q in the denominator. (Mixing lines are straight if one plots q_D versus q.) Hyperbolic mixing curves emerge on the q–δ plot when any two air masses, described by two arbitrary points q–δ space, are combined. Because of the hyperbolic shape, airmass mixing cannot produce a final state that is super-Rayleigh if the end members are not super-Rayleigh. For observations that capture mixing events, finding the intercept of (23) on a plot with an abscissa of q^{-1} (cf., Keeling 1958) gives δ_F, which identifies the water source.

Evaporation from the ocean ($S > 0$) is a special case where the source water is the infinite reservoir of vapor that is in thermodynamic equilibrium (i.e., saturated) with the ocean surface (Fig. 1e). Craig and Gordon (1965) suggested that the isotopic composition of the vapor at the liquid interface is in equilibrium with the ocean liquid for the given ocean skin temperature T_s. Therefore, evaporation is described by mixing lines that have a fixed end member with $\hat{q} = q_{\mathrm{sat}}(T_s)$ and $\hat{R} = R_{\mathrm{ocn}}/\alpha_e(T_s)$, as shown in Fig. 2 for the case of evaporation of ocean water at 300 K. In the analysis that

follows, the temperature of the evaporative source and the RH within the boundary layer are assumed and guided by observations. Evapotranspiration is also modeled this way. While kinetic and equilibrium fractionation accompanies evaporation from soil and transpiration, time mean statistics show that the isotopic composition of terrestrial fluxes is remarkably similar to that of precipitation (e.g., Zimmerman et al. 1967; Flanagan et al. 1991; Still et al. 2009).

b. Synthesis and phase diagram

The utility of the family of curves in Fig. 2 stems from having joint measurements of δ and q. This is not possible in precipitation studies where only δ is known. Further, the phase diagram provides a synopsis of the water cycle because observations are shown to reflect a history of both condensation processes (cyan curves, with displacement to the left) and mixing processes associated with sources (orange curves, with moistening to the right). Some key features of this diagram are as follows.

1) The mixing ratio can be used to determine the condensation (dew/frost point) temperature via the Clausius–Clapeyron relation [i.e., the abscissa is a temperature scale for condensation processes and the temperature dependence of equilibrium fractionation can be resolved during evaluation of (11), (12), or (13)].
2) The end member for evaporation from the ocean is given by the temperature of the evaporative source because of the temperature dependence of the equilibrium fractionation factor.
3) An end member of evapotranspired water can be distinct from the oceanic source and reflects the isotopic composition of continental precipitation for steady state conditions.
4) Values can be more depleted than predicted than in simple Rayleigh processes (i.e., super-Rayleigh) if the vapor has been exposed to fractionation more than once before precipitation is removed and is measured by α. No combination of mixing can lead to values in the lower right of the diagram.
5) Condensation processes are reversible if condensed liquid remains in isotopic (i.e., thermodynamic) equilibrium with the vapor, while Rayleigh-type processes are irreversible. This is indicated by the bulk precipitation efficiency ε.
6) The mean hydrology is described by the set of mixing processes that connect the distribution of distinct moist and dry air masses. The air masses are identified by their q–δ position, which is established by the history of different cloud processes or evapotranspiration.

The Lagrangian derivations given above are valid if the water budget closed over appropriate space and time scales (Pierrehumbert and Roca 1998; Trenberth 1999), and therefore it is useful to consider an ensemble of observations rather than a single observation. Specifically, while knowing where a single observation falls within the q–δ diagram is helpful, the hydrological system is better described by the joint probability distribution function (PDF) of all observations $p = p(q, \delta)$. Water vapor may enter or leave a particular geographic region giving rise to a quasi-steady state that is not in equilibrium (i.e., the atmosphere is not at rest), and which is described by the PDF. The moisture fluxes are related to the change in the PDF between air that enters and exits the region. The evolution of the PDF is governed by Liouville's conservation law, namely,

$$\frac{dp}{dt} = \frac{\partial p}{\partial t} + (\dot{q}, \dot{\delta}) \cdot \nabla p = 0. \tag{24}$$

Considering the dynamics of PDFs is common in studies of nonequilibrium statistics, such as found in statistical mechanics (e.g., following from Jaynes 1957b,a), and is similarly convenient for our case. In the absence of sources and sinks, the PDF of an ensemble of parcels is constant following the motion. However, PDF will change along airmass trajectories when there are moisture sources and sinks. In this case, (24) can be invoked to expose the q–δ characteristics of water sources and sinks. Specifically, changes (or divergence) in p are related to the flux q and δ, and locations of maxima in the PDF divergence reveal the (q, δ) signature of vapor associated with water sources or sinks in a geographic domain of interest.

The analysis that follows uses estimates of q and δ derived from observations to deduce which type of processes contribute to the humidity budget by matching the slope of the observed vector $(\dot{q}, \dot{\delta})$ to the theoretical trajectories in q–δ space given by (12) (logarithmic), (13) (almost linear), and (23) (hyperbolic). Lagrangian estimates of the change in p are used to identify the isotopic signature (q–δ value) of the dominant sources and sinks.

3. Data and processing

Temperature and H_2O and HDO volume mixing ratios are from TES version 4 nadir view observations (Worden et al. 2006). The error on individual HDO measurements is around 10‰ between 30°S and 30°N and increases to around 20‰ in the midlatitudes. The horizontal footprint of observations is about 5×8 km. TES version 4 data span from September 2004 to August 2008, with typically between 1000 and 3000 high-quality profiles recovered each day, which gives 888 161

individual observations from both global survey and special observation periods. The retrieval of the HDO is most sensitive to a broad layer of the atmosphere with a maximum near 700 hPa, and analysis here concentrates on mass-weighted mean values integrated between 800 and 500 hPa. The isotope ratios are the ratio of the mass-weighted mean HDO and H_2O within this layer. A discussion of the variation in sensitivity of the observations associated with clouds is given by Lee et al. (2011).

For consistency with the isotope ratio, RH is calculated as the ratio of the layer mean H_2O mixing ratio and the saturation mixing ratio at the layer mean temperature. The layer mean RH may be lower than pointwise estimates because of the temperature dependence of the saturation vapor pressure, because temperature and q retrievals have different vertical sensitivity in the TES retrievals, and because there is a known low bias in the TES q measurement (Shephard et al. 2008). Maps are constructed by binning orbit-track data onto a $5° \times 5°$ longitude–latitude grid and are smoothed with two passes of a binomial kernel.

The data quality control follows Worden et al. (2006, 2007). Retrievals that have less than 0.5 degrees of freedom and scenes with more than one unit cloud optical depth are typically lower quality and are filtered out in analysis (see discussion by Worden et al. 2007). The remaining profiles have similar vertical sensitivity. Lee et al. (2011) showed a weak dependence on the altitude of sensitivity with cloud type, but that 95% of TES scenes are either cloud free or have thin cloud. The data screening has limited influence on the results since it is the isotopic composition of interstitial water vapor rather than water in the cloudy region that is of interest to investigate the hydrologic history of air masses. The lack of interstitial water vapor measurements is a weak limitation in constructing the mean and likely results in a bias toward low humidity conditions.

The tendencies $\dot{q}$ and $\dot{\delta}$ are constructed from the difference between each observation and the value upstream along a Lagrangian back trajectory. The upstream observation is found from a backward trajectory that terminates when the trajectory point was within 120 km and 90 min of a previous TES observation. About 22% of all observations have upstream pairs between 1 and 4.5 days along the trajectory, and the choice of the 120 km target is based on the uncertainty in trajectory locations and that it is smaller than the typical length scale for large-scale flow. This criterion is a compromise between obtaining a sufficient sample size and being confident of the trajectory path. The three-dimensional kinematic back trajectories use wind fields from the Natinoal Center for Atmospheric Research (NCAR)–National Centers for Environmental Prediction (NCEP) reanalysis (Kalnay et al. 1996) and do not account for convective transport (Noone and Simmonds 1999; Noone et al. 1999). Results are largely insensitive to trajectory dispersion and the launch altitude because of coherence in the large-scale flow. Although the trajectories are three-dimensional, the TES data have only about one degree of freedom, which is taken as one layer that is 300 hPa thick. The upstream values are therefore computed as the mean retrieved H_2O and HDO values in the 300-hPa layer that is centered on the level where each back trajectory ends. Since the TES retrievals are sensitive to a lower-midtroposphere layer, some of the information about vertical variations originates in the first guess that is used in the retrieval (which is a tropical average profile derived from an isotope enabled general circulation model). While account for subsidence is made with the trajectory altitude, the vertical changes in R are poorly observed by TES. In practice this has a relatively small effect because the duration of trajectory segments are typically short relative to the time scales for subsidence. Nonetheless, one must be mindful that the results are likely biased toward horizontal considerations.

Individual observations within some geographic regions are used to construct joint PDFs in q–δ space by binning onto a grid with spacing of $\Delta q = 0.5$ mmol mol^{-1} and $\Delta\delta = 5‰$. The resulting distribution is smoothed with two applications of 3×3 point binomial kernel and normalized to ensure an integral of one. Changes in p given by (24) are found as the difference between the PDF of observations in some regions and the PDF of observations at points upstream along the back trajectories.

4. Results

The theoretical framework is used with data from regions where there is most covariability in humidity and the isotope ratio since it is in these regions where pronounced signals are anticipated. The analysis aims to first contrast regions where there are significant differences in the underlying hydrology (i.e., regions of high RH with those of low RH). The hydrological balance in the low humidity regions of each hemisphere is examined to assess the role of cloud microphysical influences on the water balance relative to a pure advection–condensation view.

a. Mean observed RH and δ distribution

Figure 3 shows the mean RH for December–February (DJF) and June–August (JJA) seasons. The figure shows the minima in the RH in the subtropics and high

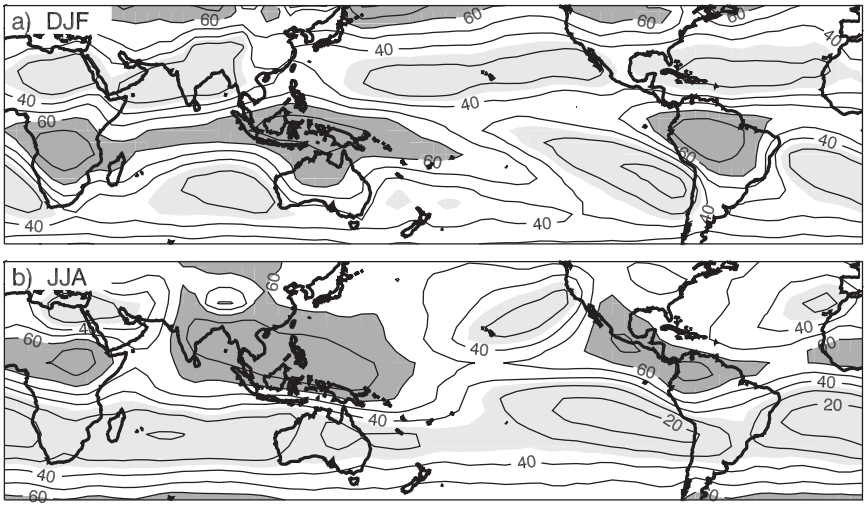

FIG. 3. Relative humidity from TES 800–500-hPa-layer mean observations for (a) DJF and (b) JJA. Values <35% have light shading, and values >60% have dark shading. The contour interval is 10%.

RH in the western tropical Pacific and over continents. Figure 4 shows the (unweighted) mean δ is similarly high in these tropical areas, particularly in monsoonal areas as noted by Brown et al. (2008). High δ values show where vapor has experienced limited condensation during transport from the source region, and thus indicate where water enters the free troposphere. Low δ value air (say, $<-250‰$) appears at higher latitudes resulting from condensation during poleward transit (Noone 2008) and in the equatorward flow on the eastern side of ocean basins associated with the mean flow of the subtropical anticyclones and with subsidence.

b. Covariation in δ and RH

The highest 25% and lowest 25% of RH values within each 5° × 5° grid cell are grouped together, and the mass-weighed mean δ values found. Figure 5 shows the difference between δ values for the high minus low RH populations and suggests different processes control relative humidity variations in different regions. The western Pacific has low δ values when the RH is high, while tropical continents have high δ when RH is high during the wet season. The continental result has been noted previously (Brown et al. 2008; Field et al. 2010)

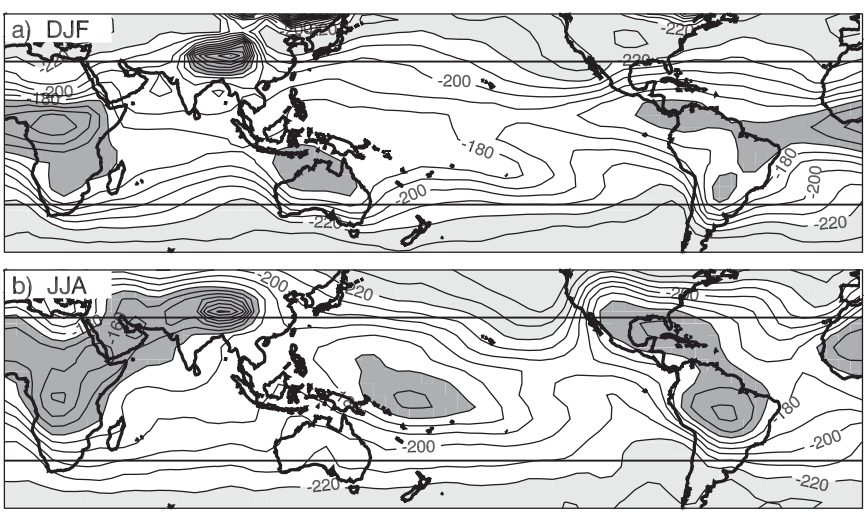

FIG. 4. Arithmetic mean δ from TES 800–500-hPa-layer mean observations for (a) DJF and (b) JJA. Values $<-220‰$ have light shading and values $>-170‰$ have dark shading. The contour interval is 10‰. Horizontal lines show 30°N and 30°S.

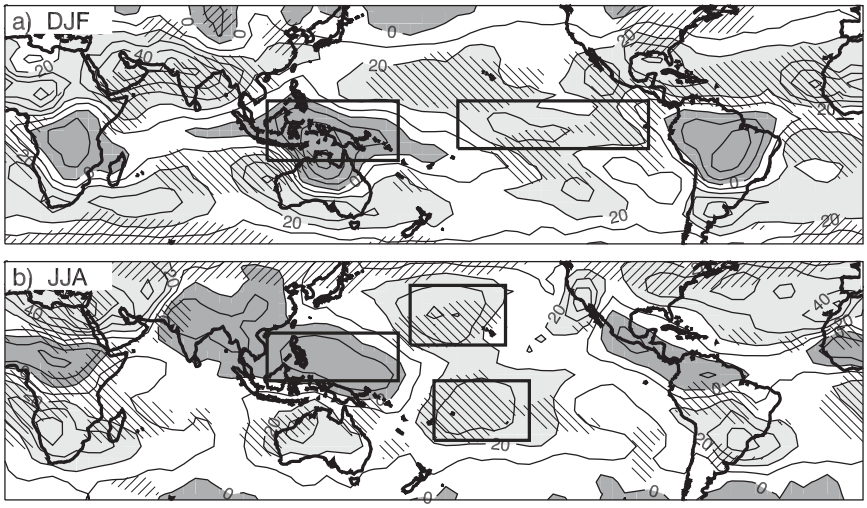

FIG. 5. Difference between δ values of highest and lowest RH quartiles for (a) DJF and (b) JJA. Negative values have dark shading and values higher than 20‰ have light shading. The contour interval is 10‰. Quartiles are based on all points within each 5° longitude by 5° latitude cell, and there are typically 250 observation points in each cell. Hatching shows where the magnitude of the correlation between δ and RH is significant at the 95% level (typically $|r| > 0.22$).

and linked to frequent deep convection. While Lee et al. (2011) showed TES observations are sensitive to higher altitudes when there are precipitating clouds, the frequency of high-quality precipitating cloud observations is low (<1% of the time), so one may be confident that the result is not primarily a sampling artifact.

Linear regression shows that for all locations the RH increases with higher water specific humidity and with lower temperature (Fig. 6). The linear relationship between the RH and specific humidity is mostly uniform geographically (i.e., same sign, and about the same magnitude). The relationship between temperature (shown as saturation mixing ratio) and RH is less uniform, with a difference in the range of values between locations where the mean RH is above 40% and those below. The temperature and specific humidity slopes in Figs. 6a and 6b follow from the definition of RH. On the other hand, the change in sign of the δ–RH slope confirms that the processes that control the high and low RH differ. Although the TES HDO retrieval is sensitive to mixing ratio and has the potential to influence this finding, the effect is weak within the tropics (Lee et al. 2011). Notice the spatial correlation between mean δ and RH is weak because of the opposing signs of the slope in Fig. 6c.

Areas with negative correlation typically coincide with regions where the mean δ values are high, which suggests convection in these areas detrain significant amounts of water vapor and are associated with rain evaporation.

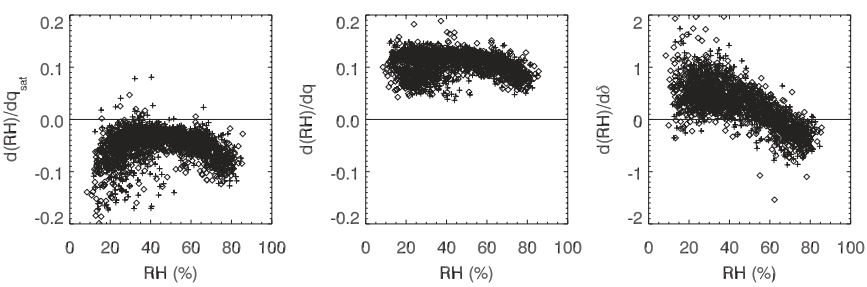

FIG. 6. Slope of linear regression between RH and (a) saturation mixing ratio, (b) mixing ratio, and (c) δ in the tropical domain between 30°S and 30°N. Units are % (mmol mol^{-1})$^{-1}$ in (a),(b) and % ‰$^{-1}$ in (c). Climatologically dry regions are associated with processes that reduce the δ value as they remove moisture, while moist locations tend to be dominated by processes that increase the δ value during dehydration. Each point results from all observations falling in each 5° × 5° bin. Data for DJF are shown with plus symbols and JJA as diamonds and indicates there is not a particularly strong seasonal bias in the tropical domain.

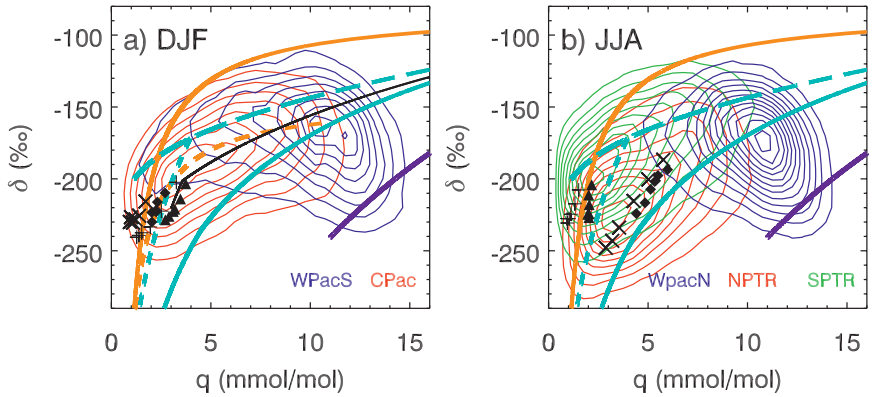

FIG. 7. Probability distribution p of observations within geographic regions identified as in Fig. 5. WPac shown in blue for southern and northern summer location, central Pacific (CPac) shown in red in (a), while NPTR is in red and SPTR is shown in green in (b). The contour interval is 2.5×10^{-3}, and the integral of each PDF is 1. Theoretical curves are those described in Fig. 2 and the text, with an additional mixing curve that shows the approximate path taken when mixing air between the high-latitude source and the most probable value found in the WPac (dashed orange). The black curve in (a) is for precipitation efficiency of 60%. Values are plotted for the mean of 5° bins from 60° to 30° latitude. Crosses show low RH quartile means and filled symbols show high RH quartile means. Northern Hemisphere data are shown as "times" symbols and filled diamonds, and Southern Hemisphere data are shown as "plus" symbol and filled triangles.

This remains to be validated using the theoretical framework. There is some evidence for lower δ values with higher RH in the midlatitudes of the winter hemisphere, which is consistent with frontal convection. However, discussion is restricted to the tropics since the accuracy of the HDO retrievals is higher and uniform within the tropics between 30°N and 30°S (Worden et al. 2006).

The eastern Pacific during DJF and locations displaced from the equator in the central Pacific during JJA show that δ values are low when the RH is low (positive correlation). The largest positive δ differences in Fig. 5 are not coincident with the locations of the subtropical RH minima seen in Fig. 3 but downstream because of the time scale of the exchange processes relative to the advective time scale. In these areas, we propose that high RH conditions are associated with the influx of vapor derived from near-complete evaporation of cloud or falling condensate (low precipitation efficiency, $\varepsilon \sim 0$), which can be tested with the theoretical framework. Since the isotopic information from a single region contains no information on the transport paths, back trajectories must be used to determine if the enriched water is local or if it is lofted into the troposphere upstream and subsequently advected to the region.

c. Bulk cloud processes

Before examining the moisture budget of the lowest humidity regions, the fluxes in the region where the RH–δ correlations are strongest are examined because the different processes are more pronounced. Figure 7 shows the joint PDF p of observations in regions defined by the boxes drawn in Fig. 5. The humidity–isotope vector components ($\dot{q}$, $\dot{\delta}$) are computed and shown in Fig. 8 as the difference between the TES q and δ at either end of the back trajectories and divided by the trajectory duration in units of days. The $\dot{q}$, $\dot{\delta}$ values are binned on the q–δ grid in two populations: those associated with parcels that have undergone diabatic heating ($\dot{\theta} >$ 0.1 K day^{-1}) and cooling ($\dot{\theta} < -0.1$ K day^{-1}). Heating rates are also computed from the difference in potential temperature θ along each trajectory and are interpolated from the NCAR–NCEP reanalysis. Although dominated by radiative and latent heating, this estimate may include influences from airmass mixing since the trajectories are computed from large-scale wind fields that include convection and mixing at the subgrid scale.

In both DJF and JJA, the western Pacific (WPacS and WPacN, where N or S denotes a meridional shift to match the seasonal change in location of most intense convection; see Fig. 5) shows low δ values at high water vapor mixing ratio values that are below the cyan Rayleigh curve, (12). Therefore modeling these data requires an effective fractionation factor with $\phi > 0$ and consequently identifies rain evaporation. Figures 8a and 8d shows that q–δ trajectory (vectors $\dot{q}$, $\dot{\delta}$) are near parallel to a super-Rayleigh curve and associated with diabatic heating associated with net moisture loss in the region. Super-Rayleigh behavior during times of high

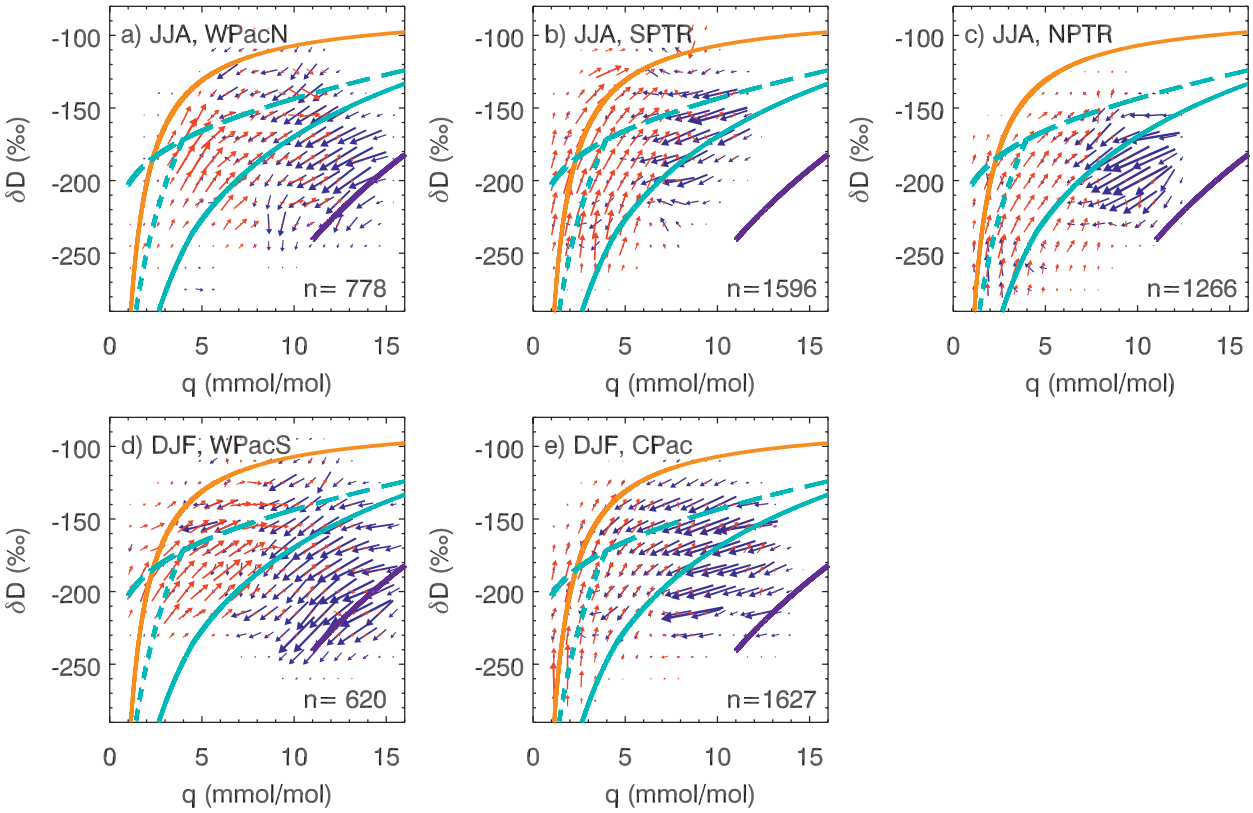

FIG. 8. Vectors defined by tendencies of q and δ along all back trajectories ending within each region identified as in Fig. 5. The vector field for observations where there has been diabatic heating ($\dot{\theta} > 0.1$ K day^{-1}) is shown in blue (moisture loss), and cooling ($\dot{\theta} < -0.1$ K day^{-1}) is in red (moisture gain). The length of the vectors indicates a change in state over a 1-day period. The total number of observations used to compile statistics is given as n in each panel and is smaller in the WPac regions because of cloud cover.

humidity explains the negative correlation between q and δ in Fig. 5. These values may be set either in situ or, more likely, in the boundary layer or within cloud systems and subsequently lofted to the altitude that TES observes. The influence of isotopic exchange during rain evaporation was noted by Worden et al. (2007) and results here suggest that rain evaporation prevails over large areas of the tropics. This finding provides observational evidence that supports earlier work that found that the remoistening of the lower troposphere by evaporation of rain and the reprocessing of water in the region of clouds is a feature of the western Pacific (e.g., Houze 1989; Lin and Johnson 1996).

Figure 8 shows evidence for reversible moist adiabatic processes in the central Pacific region (CPac). In DJF the PDF has a ridge and vectors are mostly parallel to the curve for a reversible moist adiabatic process (cf. Figs. 8d and 8e). Most of the observations lie between the (dashed) reversible moist adiabatic curve and the (solid) pseudoadiabatic Raleigh curve. Indeed a curve with precipitation efficiency of around $\varepsilon = 0.65$ (solid black curve in Fig. 7a) describes the data reasonably well, suggesting that about 65% of the condensate falls as precipitation and the remaining cloud evaporates at some time later. (If the cloud does not evaporate, that air mass is unlikely to be observed by TES.) While this estimate is not quantitatively rigorous it provides the qualitative evidence for the mechanism. Indeed it is a result that arises from the isotopic constraint and cannot be found from humidity measurements alone. A back trajectory analysis is required to determine if the water has a local origin or if it is lofted upstream and subsequently advected into the region.

Figure 7a shows a second local ridge in the CPac PDF at high mixing ratio values at around −200‰, which aligns well with a mixing line that connects the most probable value in the central Pacific with that in the western Pacific (consider dashed orange mixing curve) and suggests a distinct advective source. Following (24), the PDF of the upstream location would be imprinted downstream in the central Pacific. This provides an explanation for the central Pacific observations that are more depleted than simple distillation, which can be confirmed with back trajectories.

d. Drying and mixing processes

Figure 7 shows that lower mixing ratio values in the central Pacific may be transported in from elsewhere. Vectors associated with diabatic cooling are approximately parallel to the orange mixing line given by (23). The PDF shows an extended lobe to lower δ values between 2 to 4 mmol mol^{-1}. Also shown in Fig. 7 are the zonal (and mass weighted) mean values for each 5° latitude bin between 60° and 30° latitude, again grouped by the lowest (crosses) and highest (filled symbols) 25% of RH observations. Similarity between these higher-latitude values with the lower humidity central Pacific observations confirms intrusion of dry air into the central Pacific from high latitudes is an important control. This result must be viewed with caution because the 800–500-hPa layer observed by TES is typically lower altitude than a mean altitude of an isentrope that connects the subtropics to the midlatitudes. Nonetheless, the finding is consistent with the last saturation argument employed by Galewsky and Hurley (2010). On the other hand, similar values of q–δ pairs can also arise from dehydration within deep convection and subsequent local subsidence cannot be discounted as the dehydration mechanism.

Asymmetry between the hemispheres is evident in the contrast between the North Pacific trade region (NPTR) and the South Pacific trade region (SPTR) results, and the high-latitude observations given in Fig. 7. While the SPTR PDF aligns well with the dashed cyan curve with very low precipitation efficiency, the NPTR PDF is closer to Rayleigh (say, $\varepsilon \sim 0.8$). Similarly, the Northern Hemisphere high-latitude values in JJA are reasonably described by a Rayleigh distillation that starts from a subtropical air mass. The most humid values (filled diamonds) fall near the Rayleigh curve in a manner consistent with continual condensation during transport from lower latitude. The lowest humidity points (diagonal crosses) are also in a region of the diagram dominated by condensation processes, but because they do not fall on the Rayleigh curve it is likely they have undergone mixing or that the source of the moisture is not only the subtropical ocean (say, contributions from ocean temperature less than 25°C or land). The fact that the Northern Hemisphere stands out in this regard may be an indication of the important role that continental monsoon circulations have on the Northern Hemisphere hydrology during the boreal summer.

e. Balance of moistening and dehydration in the dry subtropics

The low humidity regions of the subtropics are distinct (recall Fig. 3) and warrant special attention. TES observations that fall within areas in each hemisphere where the seasonal mean RH is less than 35% are chosen (light shading Fig. 3) and the conditional joint q–δ PDF is constructed (conditioned on the end points of the trajectory lying within regions with mean RH $< 35\%$). As in the construction of Fig. 8, back trajectories are computed and upstream trajectory points that correspond to earlier TES observations are used to construct an upstream PDF. The difference between these two PDFs (final minus upstream) is shown in Fig. 9. Appealing to (24), divergence in the probability (blue negative contours) in the q–δ space indicates the isotopic composition of the water entering the region with both high and low humidity. Where the minima in the divergence field indicate low humidity air, entraining that air to the region will cause drying. Similarly a moisture source is indicated where the local minima indicate higher humidity air. Positive divergence (red contours) indicates the mean isotopic composition of air exiting the volume of atmosphere sampled by the trajectories. Given the limitations in the sensitivity of the TES data in low humidity scenes these divergent points are likely to have a high bias in δ.

The figure shows that the mean values in all subtropical regions are a mixture between very depleted and low humidity air and higher humidity air (dashed orange curve). The high humidity observations are broadly aligned along the Rayleigh curve, although the most probable values near 9 mmol/mol suggest typical precipitation efficiency is around $\varepsilon = 50\%$. Values below the Rayleigh curve suggest rain evaporation and consequently an equatorial origin. Indeed Fig. 10 shows the distribution of back trajectory positions four days before arrival within the low humidity region, and confirm that these high humidity observations originate equatorward and to the east of the low humidity zones. In the case of the Northern Hemisphere wintertime, the western Pacific is the upstream location of moist air as anticipated from knowing the PDF of western Pacific observations.

The source of dry air is identified in Fig. 9 at around $\delta = -300‰$ and $q = 1$–2 mmol mol^{-1}. These values can be obtained by a history of condensation in which nearly all the water mass is removed (mean $\varepsilon \approx 1$ over the length of the trajectory). Figure 10 shows the origin of these depleted values is at higher latitude. The upstream location is typically in the eastern flank of the subtropical mean anticyclones. This result is in agreement with the findings of Cau et al. (2007) and Galewsky et al. (2005) and suggests the isotopic model of Galewsky and Hurley (2010) may be a robust depiction for the dry advective control. The role of regional subsidence is likely underrepresented in this analysis because the higher-altitude δ values are likely more depleted than TES measures. Recall that although the trajectories are

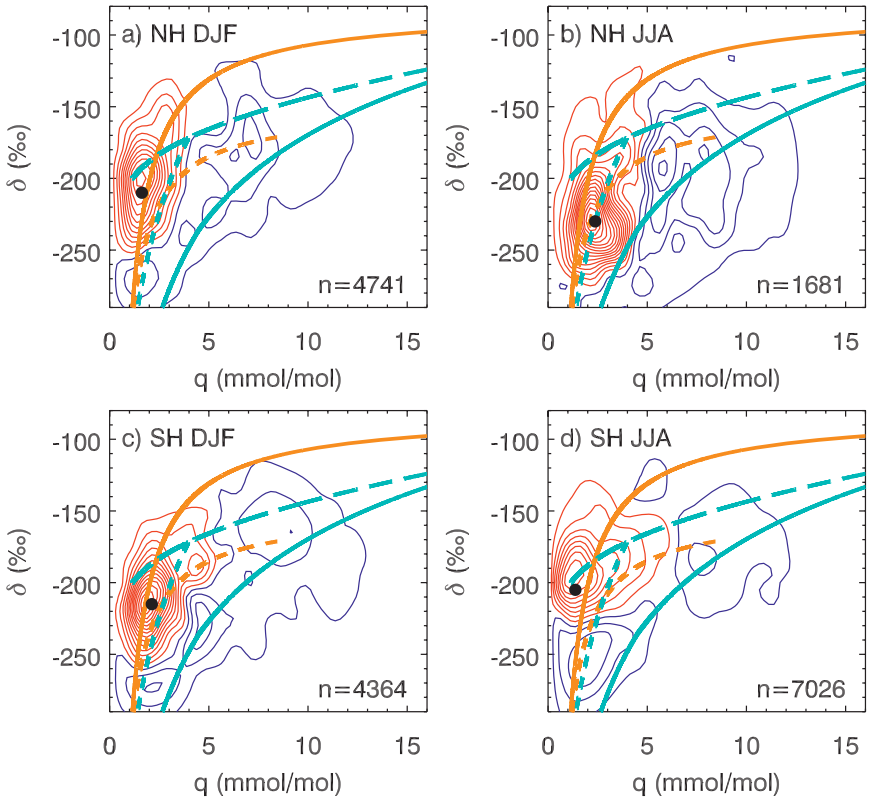

FIG. 9. Change in the PDF along back trajectories (final PDF − upstream PDF) for observations where the mean RH is less than 35%: (a) NH DJF, (b) NH JJA, (c) SH DJF, and (d) SH JJA. Negative values are contoured blue and indicate the distribution of the upstream water vapor and positive values are contoured red. The black dot shows the most probable value. The contour interval is 2.5×10^{-3}, and the 0 contour has been omitted.

three-dimensional, the layer-averaged nature of the TES data likely biases the findings toward a principally horizontal explanation.

5. Discussion

The analysis is based on similarity between the idealized trajectories (in Fig. 2) and the phase space trajectories of the TES observations in q–δ space. The theoretical models are necessarily simplistic and assume a uniform parcel temperature, specific humidity, liquid water content, and constant precipitation efficiency, which may not be a particularly precise analog for a heterogeneous 300-hPa-deep layer of the troposphere. Nonetheless, the ability of the theory to capture different features of the observed q–δ pairs is quite satisfying and suggests that some features of the atmospheric hydrology can be robustly explained in simple ways. Simple approaches to explain the distribution of atmospheric humidity without isotopic data have been shown elsewhere (e.g., Sherwood 1996b; Galewsky et al. 2005; Pierrehumbert et al. 2007; Ryoo et al. 2009), and the present results make a step toward validating these approaches with new constraints.

TES HDO measurements reveal that both the cloud processes and the dynamic controls on atmospheric humidity are important, with the former dominating over continents and in the western Pacific within the subtropical mixing barrier (Yang and Pierrehumbert 1994). The evaporation of raindrops below the cloud base with condensation at some higher elevations describes a redistribution of energy that is greater than that which results without rain evaporation. The degree to which rain evaporation enhances the large-scale divergent flow in the western Pacific is unclear, but the geographic region identified in Fig. 5 where there are negative δ differences clearly marks the regions where rainfall exchange impacts regional budgets. This gives an observational constraint on the location of the subtropical mixing barrier described by Pierrehumbert and Yang (1993) in which air (and vapor) of subtropical origin is unable to mix upstream into the convectively driven divergent flow.

In the subtropics, the variation in the TES HDO measurements suggests the dominance of a dynamic

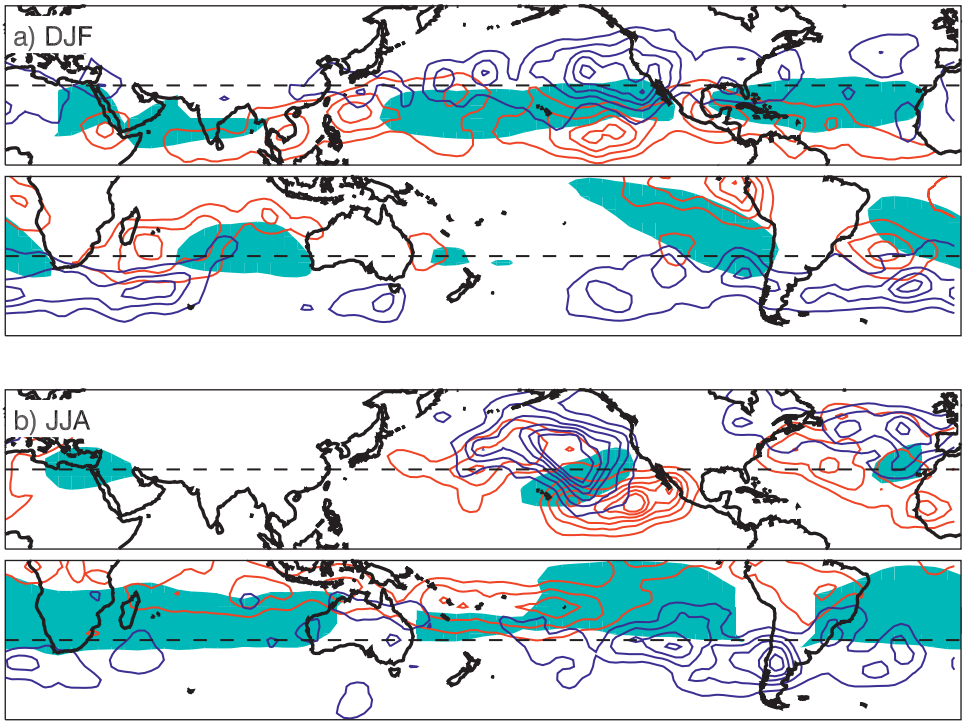

FIG. 10. Probability distributions of back trajectory positions four days prior to arrival in subtropical dry zones for (a) DJF and (b) JJA. Shading indicates seasonal mean relative humidity <35% and is the arrival region of interest. Blue contours show origin of dry end-member parcels ($q < 3$ mmol mol^{-1} and $\delta < -290‰$), and red contours indicate moist end-member parcels ($q > 5$ mmol mol^{-1} and $\delta > -250‰$). Contour interval is 5×10^{-5}, and each PDF integrates to 1. Statistics for each hemisphere are computed separately.

mechanism associated with horizontal mixing between moist filaments of tropical origin (Zhu and Newell 1994) and dry air from higher latitudes. The dry airmass intrusion is consistent with nonisotopic diagnostic studies (Galewsky et al. 2005; Schneider et al. 2006; Cau et al. 2007). The results from TES suggest that assuming isotopic composition is set via a Rayleigh process during the time of last saturation (Noone, 2008; Galewsky and Hurley 2010) may be conceptually correct, but may be quantitatively misleading because it neglects the influence of cloud condensate and microphysical processes.

The isotopic considerations extend the last saturation paradigm by identifying moistening associated with convective detrainment, which is (presumably) near saturation at the in-cloud temperature. While water vapor is expected to be processed by clouds as it travels from the boundary layer to the troposphere, using ε and α allow new insight into the type of cloud processes responsible. Couhert et al. (2010) found the vertical component of eddy moisture convergence dominates in the subtropical regions in atmospheric analysis that included parameterized moisture transport by convective clouds, which hints at a source of moisture associated with clouds. Noone (2008) similarly points out this vapor will be exported to the free troposphere by boundary layer activity and detrainment and will have undergone isotopic fractionation that accompanies precipitation. This is confirmed here by finding a principle moisture source of subtropical water vapor is associated with precipitation efficiency less than one.

Precipitation efficiency as defined here for isotopic purposes is a bulk measure of the conditions under which precipitation forms and differs somewhat from the common definitions (e.g., Sui et al. 2007). Two important cases expose the differences. First, in the isotopic model cloud condensate is assumed to be liquid. While this is appropriate for the tropical data, ice clouds formed by deposition (rather than freezing) will have $\varepsilon = 1$ even though the cloud ice may not fall out. Since cloud glaciation occurs as a function of height, it complicates attempts to infer precipitation efficiency for a given location. Second, since TES observations are mostly cloud free there is some ambiguity in whether they should be compared to modeled values for q or $q + l$. The latter is appropriate for nonprecipitating clouds

and the isotopic ratio of the final vapor will be the same as the original vapor (i.e., the total $q_0 = q + l$ is conserved). On the other hand, coalescence in clouds formed under reversible conditions will produce rain with the same isotope ratio as the cloud liquid and is the more relevant case for shallow convection. The remaining vapor will follow the expected evolution for q in a model with $\varepsilon \approx 0$ even though most of the condensate may eventually fall. These two cases illustrate that the isotopic state provides information on the microphysical behavior during previous condensation events but also that care needs to be taken in translating isotopic quantities to more conventionally defined parameters. It is likely that the full utility of isotopic information can only be realized once combined with suitably detailed process models.

From the isotope data alone, it cannot be determined if the source of water vapor associated with convective detrainment is within the dry subtropics or if the clouds are upstream and moisture is subsequently advected into the region (as, perhaps, a moist filament of equatorial origin). The classic view that the marine boundary layer acts as a material surface (e.g., Medeiros et al. 2005; Stevens et al. 2005) also posits that maintenance of the trade inversion is associated with evaporation of trade cumulus, which counteracts regional subsidence (e.g., Betts 1982), and suggests local water source. On the other hand Noone et al. (2011) combined a back-trajectory analysis with in situ observations of δ from Hawaii to show the influence of tropical water on the humidity of the subtropics during the passage of a moist filament and identified the moisture as being associated with convective cloud upstream. The back trajectory analysis here shows the subtropical moisture source is mostly equatorward of the humidity minimum, but there remains a question of the distance over which water enters and leaves the moist air mass or if advective filaments simply extrude water from the near-saturated equatorial region. Moreover, the relative role of moisture sources acting during trade conditions versus times of poleward transport due to moist filaments remains unresolved.

6. Conclusions

To analyze paired observations of humidity and water vapor isotope ratio, a theoretical framework was developed that accounts for both moistening and drying processes. The framework is based on a set of expected variations in isotopic composition that follow from different hydrologic assumptions; the resulting set of curves on a q–δ phase space diagram provides a synthesis. By combining aspects of elementary isotope physics with a more complete accounting of the relevant meteorological considerations, this framework enables the use of isotopic data to identify the processes that influence regional hydrologic balance in the tropics and subtropics. The advantage of this approach comes from having 1) paired observations of HDO and H_2O to allow the definition of a thermodynamic phase space and 2) having a large volume of data such that stationary probability distributions can be examined. The PDFs allow the theoretical framework to be applied to the mean hydrological balance rather than simply the isotopic composition of individual measurements. With a large number of observations, the evolution of joint PDFs allows the moisture sources and transport pathways to be identified. The approach is employed here to give a semiquantitative survey of the main features of the subtropical moisture budget.

From TES data the range of condensation processes is captured by the general condensation model (11) under different thermodynamic assumptions (notably, reversible moist adiabatic or pseudoadiabatic) via the precipitation efficiency parameter ε. This quantity is difficult to deduce from other observations and so not well constrained in climate models. A second parameter ϕ captures the degree of isotopic exchange as raindrops fall and equilibrate with the environment, which is also a process not well constrained. The quantitative relationship between the effective fractionation (i.e., given by ϕ) and rain evaporation cannot be determined from midtropospheric TES data alone and requires at least knowledge of the boundary layer isotopic composition. Indeed with only observations of q and δ, both ε and f cannot be simultaneously constrained. Indeed in nature it is typical that multiple processes (including mixing of different air masses, subsidence, and various forms of condensation) act simultaneously, and from both the analysis approach and the data considered here it is ultimately difficult to separate them. This highlights the need for $H_2^{18}O$ observations and improved vertical resolution in HDO datasets.

The success with which the new theoretical basis was used to determine aspects of the water balance by identifying salient features in the isotope distribution suggests that more rigorous methods are likely to be successful. Specifically, this work demonstrates that there are advantages to assimilating TES HDO data in comprehensive models to exploit the unique information provided by the isotope ratio about cloud processes and transport pathways. Similarly, the isotopic fingerprint of rain evaporation appears to be a robust feature and therefore provides a specific target for testing rain evaporation in cloud parameterizations to ensure that climate models correctly simulate the remoistening and vertical energy transport. Indeed, the observational results motivate a set

of modeling studies to test the fidelity of moist processes represented in climate models. Any comprehensive atmospheric model should be able to reproduce not just the mean isotopic value, but the set of joint probability distributions found in observations. In this regard, and in spite of possible sampling and sensitivity biases in the satellite HDO estimates, the findings present a clear set of targets to test individual processes in comprehensive atmospheric models that are equipped with isotopic tracers.

The key benefit of isotopic data in diagnostic studies is that they can both help rule out some candidate mechanisms and expose processes that require more detailed consideration. While the TES data provide insight into the large-scale mixing processes, the results suggest that higher-quality data may be required to fully constrain the microphysical controls. Indeed, to complement satellite observations, the use of highly accurate in situ time series measurements of isotope ratios above the boundary layer may ultimately be essential for both validating remote sensors and deducing the mechanisms that control change in atmospheric humidity with climate change. This may be particularly beneficial for monitoring the response of the atmospheric hydrology to changing climate.

Acknowledgments. The author is most grateful for the assistance and advice offered by John Worden and Kevin Bowman at the NASA Jet Propulsion Laboratory, who were instrumental in developing the HDO dataset. The author is indebted to Peter Blossey, Joseph Galewsky, Raymond Pierrehumbert, and the anonymous reviewers for offering insightful and helpful comments on this work during the review. This work was supported by grants from the NASA Jet Propulsion Laboratory, NASA Atmospheric Composition program (NNX08AR23G), and the NASA Energy and Water-cycle Study (07-NEWS07-0020).

REFERENCES

Betts, A. K., 1982: Saturation point analysis of moist convective overturning. *J. Atmos. Sci.,* **39,** 1484–1505.

Blossey, P. N., Z. M. Kuang, and D. M. Romps, 2010: Isotopic composition of water in the tropical tropopause layer in cloud-resolving simulations of an idealized tropical circulation. *J. Geophys. Res.,* **115,** D24309, doi:10.1029/2010JD014554.

Bony, S., and K. A. Emanuel, 2005: On the role of moist processes in tropical intraseasonal variability: Cloud–radiation and moisture–convection feedbacks. *J. Atmos. Sci.,* **62,** 2770–2789.

——, C. Risi, and F. Vimeux, 2008: Influence of convective processes on the isotopic composition (δ^{18}O and δD) of precipitation and water vapor in the tropics: 1. Radiative-convective equilibrium and Tropical Ocean–Global Atmosphere-Coupled Ocean-Atmosphere Response Experiment (TOGA-COARE) simulations. *J. Geophys. Res.,* **113,** D19305, doi:10.1029/2008JD009942.

Bretherton, C. S., P. Austin, and S. T. Siems, 1995: Cloudiness and marine boundary-layer dynamics in the Astex Lagrangian experiments. Part II: Cloudiness, drizzle, surface fluxes, and entrainment. *J. Atmos. Sci.,* **52,** 2724–2735.

Brown, D. P., J. Worden, and D. Noone, 2008: Comparison of atmospheric hydrology over convective continental regions using water vapor isotope measurements from space. *J. Geophys. Res.,* **113,** D15124, doi:10.1029/2007JD009676.

Cau, P., J. Methven, and B. Hoskins, 2007: Origins of dry air in the tropics and subtropics. *J. Climate,* **20,** 2745–2759.

Ciais, P., and J. Jouzel, 1994: Deuterium and oxygen 18 in precipitation: An isotopic model including mixed cloud processes. *J. Geophys. Res.,* **99,** 19 783–16 803.

Couhert, A., T. Schneider, J. L. Li, D. E. Waliser, and A. M. Tompkins, 2010: The maintenance of the relative humidity of the subtropical free troposphere. *J. Climate,* **23,** 390–403.

Craig, H., and L. I. Gordon, 1965: Deuterium and oxygen-18 variations in the ocean and marine atmosphere. *Proceedings of Conference on Stable Isotopes in Oceanic Studies and Paleotemperatures,* E. Tongiorgi, Ed., Laboratory of Geology and Nuclear Science, 9–130.

——, ——, and Y. Horibe, 1963: Isotopic exchange effects in the evaporation of water. 1. Low-temperature experimental results. *J. Geophys. Res.,* **68,** 5079–5087.

Dansgaard, W., 1964: Stable isotopes in precipitation. *Tellus,* **16,** 436–468.

Dessler, A. E., and S. C. Sherwood, 2003: A model of HDO in the tropical tropopause layer. *Atmos. Chem. Phys.,* **3,** 2173–2181.

Field, R. D., D. B. A. Jones, and D. P. Brown, 2010: Effects of postcondensation exchange on the isotopic composition of water in the atmosphere. *J. Geophys. Res.,* **115,** D24305, doi:10.1029/2010JD014334.

Flanagan, L. B., J. P. Comstock, and J. R. Ehleringer, 1991: Comparison of modeled and observed environmental-influences on the stable oxygen and hydrogen isotope composition of leaf water in *Phaseolus-Vulgaris L. Plant Physiol.,* **96,** 588–596.

Galewsky, J., and J. V. Hurley, 2010: An advection-condensation model for subtropical water vapor isotopic ratios. *J. Geophys. Res.,* **115,** D16116, doi:10.1029/2009JD013651.

——, A. Sobel, and I. Held, 2005: Diagnosis of subtropical humidity dynamics using tracers of last saturation. *J. Atmos. Sci.,* **62,** 3353–3367.

Gat, J. R., 1996: Oxygen and hydrogen isotopes in the hydrologic cycle. *Annu. Rev. Earth Planet. Sci.,* **24,** 225–262.

——, 2000: Atmospheric water balance—The isotopic perspective. *Hydrol. Processes,* **14,** 1357–1369.

Gedzelman, S. D., 1988: Deuterium in water vapour above the atmospheric boundary layer. *Tellus,* **40B,** 134–147.

He, H., and R. B. Smith, 1999a: Stable isotope composition of water vapor in the atmospheric boundary layer above the forests of New England. *J. Geophys. Res.,* **104,** 11 657–11 673.

——, and ——, 1999b: An advective-diffusive isotopic evaporation-condensation model. *J. Geophys. Res.,* **104,** 18 619–18 630.

Hoffmann, G., M. Werner, and M. Heimann, 1998: Water isotope module of the ECHAM atmospheric general circulation model: A study on timescales from days to several years. *J. Geophys. Res.,* **103,** 16 871–16 896.

Houze, R. A., 1989: Observed structure of mesoscale convective systems and implications for large-scale heating. *Quart. J. Roy. Meteor. Soc.,* **115,** 425–461.

Hurley, J. V., and J. Galewsky, 2010: A last-saturation diagnosis of subtropical water vapor response to global warming. *Geophys. Res. Lett.,* **37,** L06702, doi:10.1029/2009GL042316.

Jaynes, E. T., 1957a: Information theory and statistical mechanics. *Phys. Rev.,* **106,** 620–630.

——, 1957b: Information theory and statistical mechanics. 2. *Phys. Rev.,* **108,** 171–190.

Jouzel, J., 1986: Isotopes in cloud physics: Multistep and multistage processes. *Handbook of Environmental Isotope Geochemistry,* Vol. 2, *The Terrestrial Environment B,* P. Fritz and J. C. Frontes, Eds., Elsevier, 61–112.

Kalnay, E., and Coauthors, 1996: The NCEP/NCAR 40-Year Reanalysis Project. *Bull. Amer. Meteor. Soc.,* **77,** 437–471.

Keeling, C. D., 1958: The concentration and isotopic abundances of atmospheric carbon dioxide in rural areas. *Geochim. Cosmochim. Acta,* **13,** 322–334.

Lawrence, J. R., and Coauthors, 2004: Stable isotopic composition of water vapor in the tropics. *J. Geophys. Res.,* **109,** D06115, doi:10.1029/2003JD004046.

Lee, J.-E., and I. Fung, 2008: ''Amount effect'' of water isotopes and quantitative analysis of post-condensation processes. *Hydrol. Processes,* **22,** 1–8.

——, ——, D. J. DePaolo, and C. C. Henning, 2007: Analysis of the global distribution of water isotopes using the NCAR atmospheric general circulation model. *J. Geophys. Res.,* **112,** D16306, doi:10.1029/2006JD007657.

——, and Coauthors, 2011: Relating tropical ocean clouds to moist processes using water vapor isotope measurements. *Atmos. Chem. Phys.,* **11,** 741–752.

Lin, X., and R. H. Johnson, 1996: Heating, moistening, and rainfall over the western Pacific warm pool during TOGA COARE. *J. Atmos. Sci.,* **53,** 3367–3383.

Medeiros, B., A. Hall, and B. Stevens, 2005: What controls the mean depth of the PBL? *J. Climate,* **18,** 3157–3172.

Merlivat, L., and J. Jouzel, 1979: Global climatic interpretation of the deuterium–oxygen-18 relationship for precipitation. *J. Geophys. Res.,* **84,** 5029–5033.

Newell, R. E., N. E. Newell, Y. Zhu, and C. Scott, 1992: Tropospheric rivers—A pilot-study. *Geophys. Res. Lett.,* **19,** 2401–2404.

Noone, D., 2008: The influence of midlatitude and tropical overturning circulation on the isotopic composition of atmospheric water vapor and Antarctic precipitation. *J. Geophys. Res.,* **113,** D04102, doi:10.1029/2007JD008892.

——, and I. Simmonds, 1999: A three-dimensional spherical trajectory algorithm. Research activities in atmospheric and oceanic modelling, World Meteorological Organization Rep. 28 WMO/TD-No. 942, 943.926–943.927.

——, and ——, 2002: Associations between δ^{18}O of water and climate parameters in a simulation of atmospheric circulation for 1979–95. *J. Climate,* **15,** 3150–3169.

——, and C. Sturm, 2010: Comprehensive dynamical models of global and regional water isotope distributions. *Isoscapes: Understanding Movement, Pattern, and Process on Earth through Isotope Mapping,* J. West et al., Eds., Springer, 195–220.

——, J. Turner, and R. Mulvaney, 1999: Atmospheric signals and characteristics of accumulation in Dronning Maud Land, Antarctica. *J. Geophys. Res.,* **104,** 19 191–19 211.

——, and Coauthors, 2011: Synoptic and diurnal influences on water vapor and air mass mixing in the subtropical atmosphere from isotopic composition measurements on Mauna Loa. *J. Geophys. Res.,* **116,** D22113, doi:10.1029/2011JD015773.

Payne, V. H., D. Noone, A. Dudhia, C. Piccolo, and R. G. Grainger, 2007: Global satellite measurements of HDO and implications for understanding the transport of water vapour into the stratosphere. *Quart. J. Roy. Meteor. Soc.,* **133,** 1459–1471.

Pierrehumbert, R. T., and H. Yang, 1993: Global chaotic mixing on isentropic surfaces. *J. Atmos. Sci.,* **50,** 2462–2480.

——, and R. Roca, 1998: Evidence for control of Atlantic subtropical humidity by large scale advection. *Geophys. Res. Lett.,* **25,** 4537–4540.

——, H. Brogniez, and R. Roca, 2007: On the relative humidity of earth's atmosphere. *The Global Circulation of the Atmosphere: Phenomena, Theory, Challenges,* T. Schneider and A. H. Sobel, Eds., Princeton University Press, 143–185.

Rayleigh, L., 1902: On the distillation of binary mixtures. *Philos. Mag.,* **4,** 521–537.

Risi, C., S. Bony, and F. Vimeux, 2008: Influence of convective processes on the isotopic composition (δ^{18}O and δD) of precipitation and atmospheric water in the tropics. Part 2: Physical interpretation of the amount effect. *J. Geophys. Res.,* **113,** D19306, doi:10.1029/2008JD009943.

Rozanski, K., L. Araguas-Araguas, and R. Gonfiantini, 1992: Relation between long-term trends of oxygen-18 isotope composition of precipitation and climate. *Science,* **258,** 981–985.

Ryoo, J. M., T. Igusa, and D. W. Waugh, 2009: PDFs of tropical tropospheric humidity: Measurements and theory. *J. Climate,* **22,** 3357–3373.

Salathe, E. P., and D. L. Hartmann, 1997: A trajectory analysis of tropical upper-tropospheric moisture and convection. *J. Climate,* **10,** 2533–2547.

Sayres, D. S., and Coauthors, 2010: Influence of convection on the water isotopic composition of the tropical tropopause layer and tropical stratosphere. *J. Geophys. Res.,* **115,** D00J20, doi:10.1029/2009JD013100.

Schneider, T., K. L. Smith, P. A. O'Gorman, and C. C. Walker, 2006: A climatology of tropospheric zonal-mean water vapor fields and fluxes in isentropic coordinates. *J. Climate,* **19,** 5918–5933.

——, P. A. O'Gorman, and X. J. Levine, 2010: Water vapor and the dynamics of climate changes. *Rev. Geophys.,* **48,** RG3001, doi:10.1029/2009RG000302.

Sharp, Z., 2006: *Principles of Stable Isotope Geochemistry.* Prentice Hall, 360 pp.

Shephard, M. W., and Coauthors, 2008: Comparison of tropospheric emission spectrometer nadir water vapor retrievals with in situ measurements. *J. Geophys. Res.,* **113,** D15S24, doi:10.1029/2007JD008822.

Sherwood, S. C., 1996a: Maintenance of the free-tropospheric tropical water vapor distribution. Part I: Clear regime budget. *J. Climate,* **9,** 2903–2918.

——, 1996b: Maintenance of the free-tropospheric tropical water vapor distribution. Part II: Simulation by large-scale advection. *J. Climate,* **9,** 2919–2934.

——, R. Roca, T. M. Weckwerth, and N. G. Andronova, 2010: Tropospheric water vapor, convection, and climate. *Rev. Geophys.,* **48,** RG2001, doi:10.1029/2009rg000301.

Stevens, B., and Coauthors, 2005: Evaluation of large-eddy simulations via observations of nocturnal marine stratocumulus. *Mon. Wea. Rev.,* **133,** 1443–1462.

Stewart, M. K., 1975: Stable isotope fractionation due to evaporation and isotopic exchange of falling waterdrops: Applications to atmospheric processes and evaporation of lakes. *J. Geophys. Res.,* **80,** 1133–1146.

Still, C. J., and Coauthors, 2009: Influence of clouds and diffuse radiation on ecosystem-atmosphere CO_2 and $CO^{18}O$ exchanges. *J. Geophys. Res.,* **114,** G01018, doi:10.1029/02007JG000675.

Sui, C. H., X. F. Li, and M. J. Yang, 2007: On the definition of precipitation efficiency. *J. Atmos. Sci.,* **64,** 4506–4513.

Trenberth, K. E., 1999: Atmospheric moisture recycling: Role of advection and local evaporation. *J. Climate,* **12,** 1368–1381.

Wen, X. F., X. M. Sun, S. C. Zhang, G. R. Yu, S. D. Sargent, and X. Lee, 2008: Continuous measurement of water vapor D/H and O-18/O-16 isotope ratios in the atmosphere. *J. Hydrol.,* **349,** 489–500.

Worden, J., and Coauthors, 2006: Tropospheric emission spectrometer observations of the tropospheric HDO/H2O ratio: Estimation approach and characterization. *J. Geophys. Res.,* **111,** D16309, doi:10.1029/2005JD006606.

——, D. Noone, and K. Bowman, 2007: Importance of rain evaporation and continental convection in the tropical water cycle. *Nature,* **445,** 528–532.

Wright, J. S., A. H. Sobel, and G. A. Schmidt, 2009: Influence of condensate evaporation on water vapor and its stable isotopes in a GCM. *Geophys. Res. Lett.,* **36,** L12804, 128, doi:10.11029/12009gl038091.

Yang, H., and R. T. Pierrehumbert, 1994: Production of dry air by isentropic mixing. *J. Atmos. Sci.,* **51,** 3437–3454.

Yoshimura, K., M. Kanamitsu, D. Noone, and T. Oki, 2008: Historical isotope simulation using reanalysis atmospheric data. *J. Geophys. Res.,* **113,** D19108, doi:10.1029/2008JD010074.

Zhu, Y., and R. E. Newell, 1994: Atmospheric rivers and bombs. *Geophys. Res. Lett.,* **21,** 1999–2002.

——, and ——, 1998: A proposed algorithm for moisture fluxes from atmospheric rivers. *Mon. Wea. Rev.,* **126,** 725–735.

Zimmerman, U., D. Ehhalt, and K. O. Munnich, 1967: Soil movement and evapotranspiration change in the isotopic composition of the water. *Proc. Symp. on Isotopes in Hydrology,* Vienna, Austria, International Atomic Energy Agency, 567–585.